Journal of Alloys and Compounds 502 (2010) 63–67

Contents lists available at ScienceDirect

Journal of Alloys and Compounds

journal homepage: www.elsevier.com/locate/jallcom

Effect of wheel speed on the microstructures and magnetic properties of rapidly solidified Sm–Co alloys

S. Aich [a,*], J.E. Shield [b]

[a] Department of Metallurgical & Materials Engineering, Indian Institute of Technology, Kharagpur 721302, West Bengal, India
[b] Department of Mechanical Engineering and Nebraska Center for Materials and Nanoscience, N104, WSEC, University of Nebraska, Lincoln, NE 68588, United States

ARTICLE INFO

Article history:
Received 17 January 2009
Received in revised form 9 April 2010
Accepted 22 April 2010
Available online 2 June 2010

Keywords:
Permanent magnets
Metals
Magnetic measurements

ABSTRACT

Melt-spinning of $Sm_{11}Co_{89}$ alloys modified with Nb and C resulted in the formation of the metastable (1:7) structure irrespective of the variations in wheel speed (20–60 m/s), with the formation of fcc-Co phase observed at $v = 60$ m/s. At higher wheel speed the higher chances of formation of Co precipitate and the reduced size of Co precipitates helped to improve the remanence. Moreover, wheel speeds up to 50 m/s resulted in refined (1:7) grain sizes and thus resulted in higher coercivity. At extremely high wheel speed ($v = 60$ m/s), short contact time with the wheel for the molten pool caused in-flight annealing and thus resulted in coarser grain and lower coercivity value. Most of the alloys exhibited a high reduced remanence ratio (~0.7) indicating significant exchange–spring interactions between the grains. At higher wheel speed the magnetization process was dominated by pinning mechanism.

1. Introduction

Rapidly solidified Sm–Co-based alloys have often exhibited improved microstructures and better magnetic properties. These kind of magnets are getting much more attention since the last decade because of their interesting features, such as high energy density (14–30 MGOe), reliable coercive force, high anisotropy, remarkable corrosion-oxidation resistance and the best temperature characteristics of any rare-earth permanent magnet, which make them the ideal material in applications, such as pump couplings, sensors and servo-motors. Rapid solidification by single-roller melt-spinning at a low wheel speed of 5 m/s produced anisotropic $SmCo_5$ ribbons which exhibited high energy product $(BH)_{max}$ as high as 18.2 MGOe and a remanence ratio of 0.9 [1–3]. Rapidly solidified $Sm(Co_{0.68}Fe_{0.22}Cu_{0.08}Zr_{0.02})_{7.7}$ magnets melt spun at lower wheel velocity (~5 m/s) exhibited higher anisotropy and better remanent magnetization ($M_r \sim 8.5$ kG) compared to the ribbons melt spun at higher wheel velocity (~40 m/s) [4]. Here reduced crystallographic texture was observed at higher wheel speed due to significant increase in the formation of isotropic $TbCu_7$-type Sm_2Co_{17} phases. The same effect was observed in $Sm(Co_{0.74}Fe_{0.1}Zr_{0.04}Cu_{0.12})_{8.5}$ ribbons, melt spun at 5 m/s, due to Zr and Cu substitution for Co [5]. Microstructural varieties were obtained in rapidly quenched $Sm(Co,Fe,Cu,Zr)_8$ ribbons by adjusting the wheel velocity [6]. The ribbons melt spun at lower velocity (below 40 m/s) exhibited lower intrinsic coercivity ($_iH_c \sim 1$ kOe) and larger grain sizes in the as-spun state, whereas, the ribbons spun at the velocities above 40 m/s were nanocrystalline and the coercivity was as high as 7 kOe. The effect of different wheel speeds (10–70 m/s) were also observed for rapidly solidified boron-substituted $Sm(Co_{0.74-x}Fe_{0.1}Cu_{0.12}Zr_{0.04}B_x)_{7.5}$ ($x = 0.005$–0.05) alloys [7]. The best magnetic properties (coercivity as high as 38.5 kOe, the reduced remanence $M_r/M_s > 0.8$) were reported for the as-spun ribbon with $x = 0.04$ at 39 m/s in which nanograins of 40–80 nm size were observed.

Some significant effects of cooling rate were also observed in several other alloy systems. In Al/Ge substituted FINEMET alloys, higher wheel velocity and higher super-heat during melt-spinning helped to produce the rapidly solidified ribbons with higher amorphicity/higher coercivity but with lower magnetic saturation and lower initial magnetic permeability [8]. In Nd–Fe–C–(B) system or $Nd_2Fe_{14}B/\alpha$-Fe nanocomposite, a more uniform structure, a stronger exchange coupling interaction and a better magnetic properties reaching a maximum value: $_iH_c = 5.5$ kOe, $J_r = 10.8$ kG, $(BH)_{max} = 14.44$ MGOe were obtained by using a specific range of wheel speed or an optimum wheel speed of 12 m/s [9,10]. By using controlled melt solidification (CMS) method, a uniform microstructure of α-Fe/$Nd_2Fe_{14}B$ nanocomposites with an average grain size of about 14 nm was obtained at a wheel speed of 20 m/s, which is not feasible at all by annealing the amorphous $Nd_{3.6}Pr_{5.4}Fe_{83}Co_3B_5$ alloy [11]. The formation of such a fine and uniform microstructure is due to the effect of the degree of undercooling of the

* Corresponding author.
E-mail addresses: saich@metal.iitkgp.ernet.in, shampa12004@yahoo.com (S. Aich).

0925-8388/$ – see front matter © 2010 Elsevier B.V. All rights reserved.
doi:10.1016/j.jallcom.2010.04.126

melt on both the nucleation and growth rates of the α-Fe and $Nd_2Fe_{14}B$ crystals. The α-Fe/$Nd_2Fe_{14}B$ nanocomposites made by CMS show good magnetic properties: $M_r/M_s = 0.74$, $H_c = 5.652$ kOe, and $(BH)_{max} = 24.4$ MGOe. The magnetic properties (H_c, M_r/M_s and $(BH)_{max}$) of as-quenched and annealed $Nd_{12}Fe_{71.4-x}Co_{10}B_{6.6}Ga_x$ ribbons at $x = 0.6$ increase with increasing wheel speed (v) and reach a maximum at $v = 25$ m/s and then decrease [12]. At the lower wheel speed ($v = 25$ m/s), the coarser grain size resulted in the smaller H_c, M_r/M_s and $(BH)_{max}$ of the films. At the highest wheel speed of $v = 30$ m/s, H_c, M_r/M_s and $(BH)_{max}$ of the as-quenched ribbons drastically decrease due to the existence of amorphous structure in the over-quenched ribbons. After annealing, H_c, M_r/M_s and $(BH)_{max}$ are all increased because of the phase transformation from amorphous into crystalline structure. The optimum grain size (~20 nm) and the best magnetic properties ($M_r/M_s = 0.73$, $(BH)_{max} = 20.3$ MGOe) were obtained for Pr–Fe–B, PrFeB-based/α-Fe and PrFeB-based/α-Fe nanocomposite melt-spun ribbons by using the optimum quenching rate by adjusting the wheel speed during rapid solidification followed by an optimum condition for subsequent annealing [13–17]. The evolution of phase formation of the melt-spun ribbons during post-annealing was highly dependent on the as-quenched structures of the ribbons.

In this present research we report about the effect of various wheel speeds on the microstructures and the magnetic properties of rapidly solidified simple binary Sm–Co alloys modified with Nb and C.

2. Experimental procedure

Alloys with a nominal composition of $(Sm_{0.11}Co_{0.89})_{94}Nb_3C_3$ were made from high-purity (>99.95%) elements by arc melting in a high-purity argon atmosphere. Before arc melting 5% extra Sm was added to the sample to compensate for the weight loss due to Sm vaporization during arc melting. To observe the effect of wheel speed on the structural and the magnetic properties the ingot was rapidly solidified by melt-spinning in presence of high-purity argon at a chamber pressure of 1 atm and at five different tangential wheel velocities of 20, 30, 40, 50 and 60 m/s.

The samples were then analyzed by X-ray diffraction using a Philips X-ray diffractometer with Cu Kα radiation. The powdered samples were mounted on an off-cut SiO_2 single crystal to avoid the diffraction effects of the sample holder, or an amorphous SiO_2 slide. Transmission electron microscopy was accomplished with a JEOL2010 operating at 200 kV. Electron transparency was achieved by mounting the melt-spun ribbon on a slightly polished Cu oval and by ion milling to perforation using a Gatan Duomill or PIPS at 4.5 kV. The magnetic measurements were made by SQUID magnetometry at 300 K utilizing a Quantum Design MPMS with maximum field of 7 T. Magnetic measurements were made on several ribbon pieces mounted so that the magnetic field was applied in the plane of the ribbon. Both X-ray diffraction and in- and out-of-plane magnetic measurement revealed an isotropic grain arrangement [18].

3. Results and discussion

X-ray diffraction patterns revealed only peaks indexing to the disordered $TbCu_7$-type $SmCo_7$ structure for wheel speeds up to 50 m/s, and the material had isotropic grain structures [18]. At 60 m/s, the diffraction pattern revealed the presence of fcc-Co along with the $SmCo_7$. The equilibrium ordered Sm_2Co_{17} with the Th_2Zn_{17}-type structure can be distinguished from the disordered $TbCu_7$-type structure by the presence of superlattice peaks. The most prominent superlattice peak for the Sm_2Co_{17} structure is the (0 2 4), which would appear at approximately 38.5° 2θ [19]. In Fig. 1 the absence of the superlattice reflections indicates that the structure is disordered. Fig. 2 shows a systematic shift in peak position with wheel speed for the (1 1 0) peak, indicating a change in lattice parameter. Lattice parameter determination using Rietveld refinement revealed an increase in "a" and a decrease in "c" as the wheel speed increased. The overall volume change was ~2.4%. Fig. 3 shows the change in "c/a" ratio with increase in wheel speed. The change in lattice parameter as a function of wheel speed shown here is opposite of what was observed for binary Sm–Co alloys as a function of wheel speed. In the binary alloys, a decrease in the "a" lattice parameter and increase in the "c" lattice parameter was observed [20], which was attributed to increased dumbbell disordering as the wheel speed increased. This opposite trend in the lattice parameters with increasing wheel speed may be caused by an increased

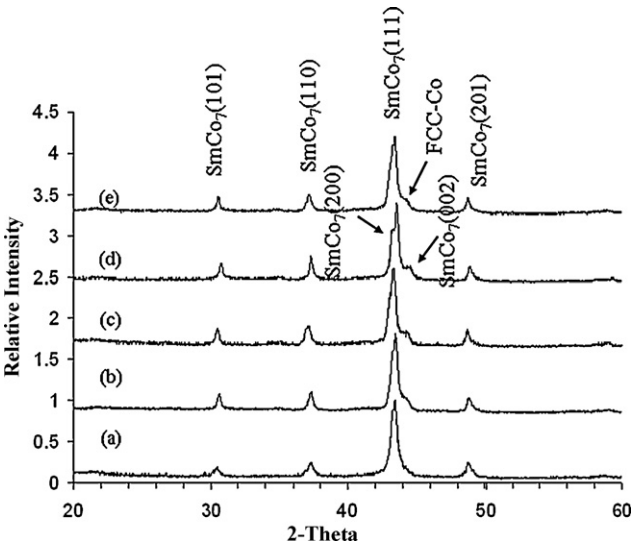

Fig. 1. X-ray diffraction scans of the $(Sm_{11}Co_{89})_{94}Nb_3C_3$ alloys with different wheel speeds: (a) 20 m/s, (b) 30 m/s, (c) 40 m/s, (d) 50 m/s and (e) 60 m/s. Peaks were indexed to the $TbCu_7$-type $SmCo_7$ structure.

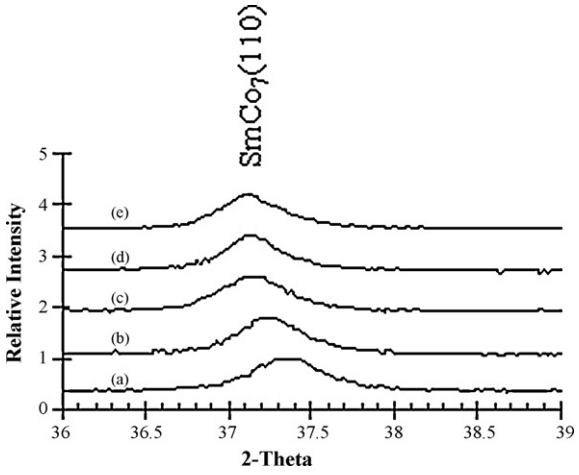

Fig. 2. X-ray diffraction scans of the $(Sm_{11}Co_{89})_{94}Nb_3C_3$ alloys with different wheel speeds: (a) 20 m/s, (b) 30 m/s, (c) 40 m/s, (d) 50 m/s and (e) 60 m/s, showing the (1 1 0) peak shift.

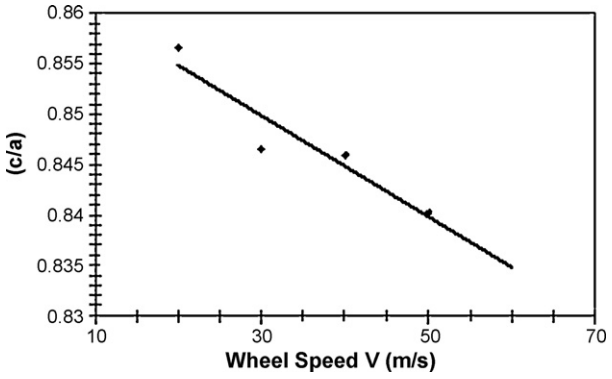

Fig. 3. Relationship between the "c/a" ratios and the wheel speed for the Sm–Co–Nb–C samples.

level of solute trapping of Nb and/or C that is a function of solidification rate (wheel speed). High-resolution X-ray diffraction patterns and Rietveld refinement of the patterns indicated that no NbC was present in rapidly solidified Sm–Co–Nb–C [21]. Also, the presence of transition metals such as Nb or Ti and C in solid solution was shown to inhibit the development of long-range order in isostructural Sm–Fe alloys, as the ordering transformation was suppressed until the precipitation of NbC or TiC occurred [22,23]. Typically, the degree of solute trapping is related to solidification velocity, which in melt-spinning is related to the wheel speed [24]. Thus, at high wheel speeds more of the Nb and C are in solution as opposed to segregated to grain boundaries. Chemical analysis using X-ray energy dispersive spectroscopy of different melt-spun samples and across grain boundaries would confirm this analysis,

Varying the wheel speed also had a significant impact on the scale of the microstructure. At 20 m/s, the microstructure consisted of equiaxed grains on the order of 150 nm (Fig. 4(a)). The grain size decreased with increasing wheel speed through 50 m/s, and then increased slightly for the sample melt spun at 60 m/s (Figs. 4 and 5). The increase in grain size at 60 m/s can be explained by the fact that at such a high wheel speed, the ribbon has a very short contact time with the wheel. As a result, the ribbon is still at an elevated temperature when it leaves the wheel, and further cooling is by convection. The relatively slower cooling allows some grain growth to occur during flight (so-called "in-flight annealing"). Alternatively, at high wheel speeds the melt-pool stability may be deleteriously affected by, for example, system vibrations. This would also influence the solidification process and lead to the anomalous grain size at 60 m/s. It should be mentioned that solidification still occurs during the contact time with the wheel, given the still fine scale of the microstructure and the formation of fcc-Co, which suggests a higher undercooling at 60 m/s and which forms as a result of non-equilibrium effects on the phase relationships [18,20].

The possibility of getting Co precipitates on the wheel contact side as well as on the free side of the melt-spun ribbons depends on the cooling rate or the speed of the copper wheel during rapid solidification. According to Fig. 6, the X-ray diffraction peaks of the wheel contact side of the ribbons are broader than the peaks from the free side of the ribbons. The relatively larger peak width in the wheel contact side X-ray diffraction pattern of the melt-spun ribbon indicates the presence of smaller grains on that side of the ribbons. The calculated grain sizes (by using Scherrer formula) were ~55 nm and ~100 nm for wheel contact side and the free side of the ribbon respectively. Also, a more prominent or distinguishable fcc-Co shoulder is visible in wheel contact side X-ray diffraction pattern than in free side X-ray diffraction pattern, which indicates the higher possibility of getting Co precipitates in the wheel contact side of the ribbon due to faster cooling rate during rapid solidification processing.

The magnetic behavior reflected the changes in the scale of the microstructure, with coercivity increasing with decreasing grain size with a $1/d$ relationship (d is the grain size) (Fig. 7). The coercivity of the sample melt spun at 60 m/s fit in well with respect to grain size, indicating that the fcc-Co present in this sample did not substantially decrease the coercivity relative to the other samples. This is likely due to the nanometer scale of the Co, which enabled it to effectively couple with the hard magnetic grains. Other work has also demonstrated an inverse relationship between coercivity and grain size in Sm–Co alloys [25,26], but these were for grain sizes that exceeded the single-domain limit (~0.7–1 μm). Here, we show that this relationship extends to single-domain grains. The magnetization process was mostly nucleation dominated except at higher wheel velocity where very slight pinning-like character was observed (Fig. 8). At lower wheel speed the magnetization curves show steeper gradient which indicates the higher initial susceptibility. This indicates that the magnetization process in the samples

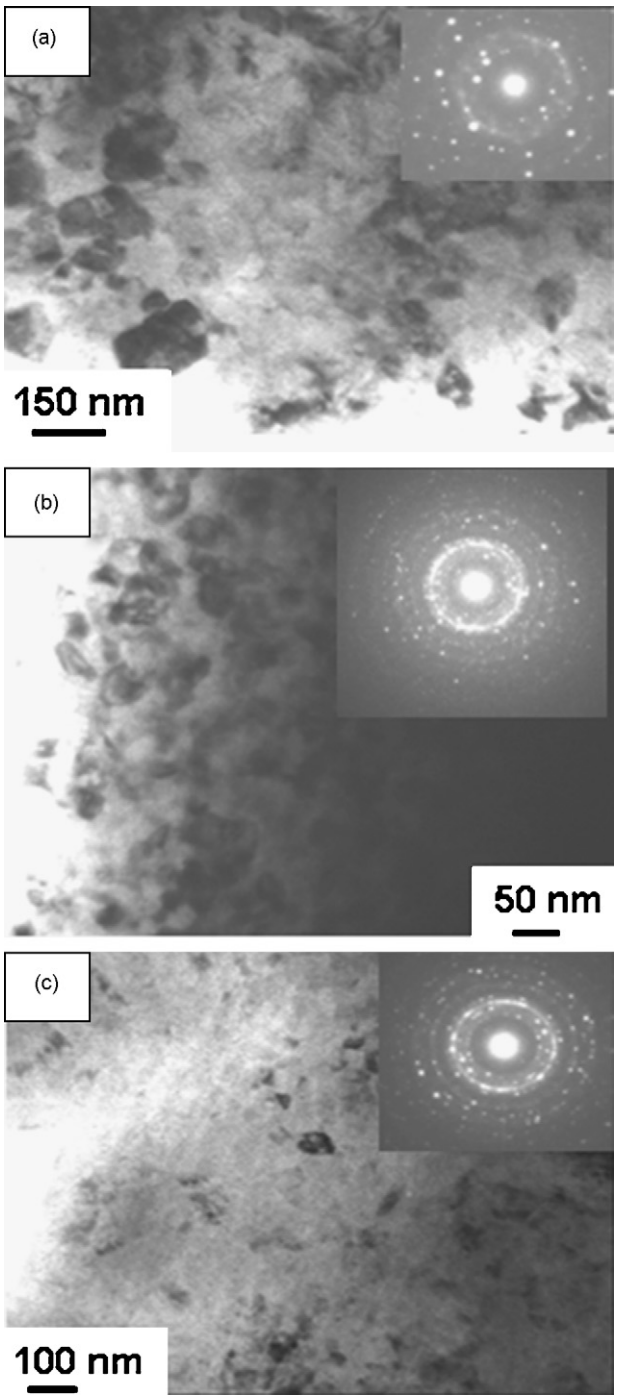

Fig. 4. Transmission electron micrographs showing the microstructures of Sm–Co–Nb–C alloys melt spun at (a) 20 m/s, (b) 40 m/s and (c) 50 m/s. The insets show the corresponding electron diffraction patterns.

melt spun at lower wheel velocity was controlled by the nucleation mechanism. The observation of a steep response in initial magnetization curves is consistent with initial magnetization by nucleation processes [27–30]. At higher wheel velocity, the flatter part of the curve with lower initial susceptibility indicates the very slight pinning-like character of the magnetization curve.

Most of the alloys (except the alloy melt spun at 40 m/s) also showed a very high remanence ratio of 0.7 suggesting exchange–spring interactions between grains. The magnetic properties, as well as the grain sizes of the various alloys, are summarized in Table 1.

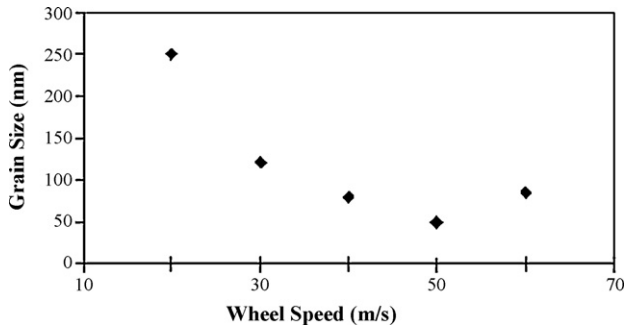

Fig. 5. Relationship between the grain size and the wheel speed of the Sm–Co–Nb–C alloys.

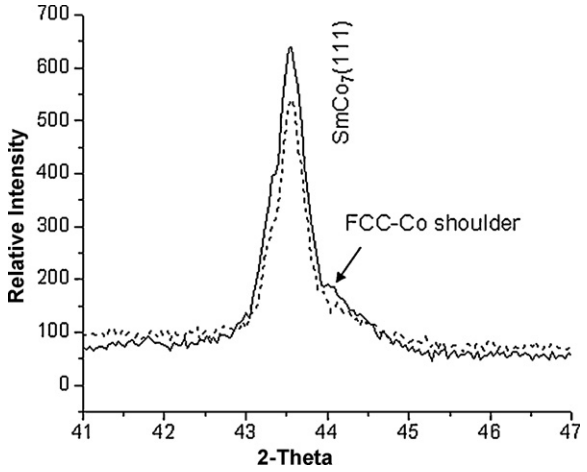

Fig. 6. X-ray diffraction pattern of the $(Sm_{11}Co_{89})_{94}Nb_3C_3$ melt-spun ribbon in the free side of the ribbon (- - -) as well as in the wheel contact side of the ribbon (—).

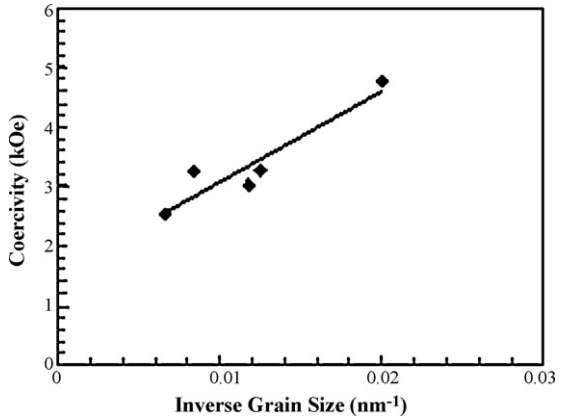

Fig. 7. Relationship between the coercivity and inverse grain size for the Sm–Co–Nb–C samples.

Table 1
Grain size and magnetic properties of the Sm–Co alloys modified with Nb and C as a function of wheel speed.

Wheel speed, v (m/s)	Grain size (nm)	Coercivity (kOe)	Remanence (kG)	Energy product (MGOe)
20	150	2.51	7.71	5.41
30	120	3.27	7.01	5.93
40	80	3.28	7.00	5.60
50	50	4.77	6.30	6.14
60	85	3.01	7.43	5.22

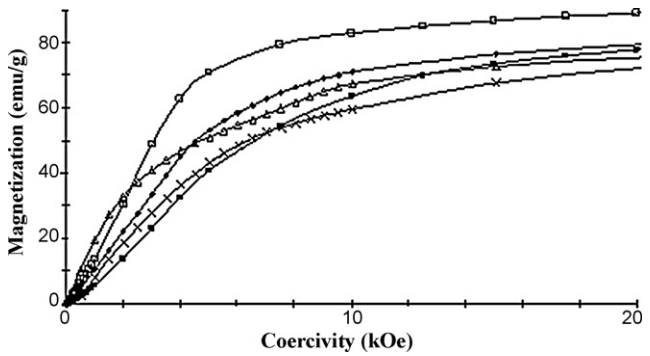

Fig. 8. The normalised curves showing initial magnetization processes for the $(Sm_{11}Co_{89})_{94}Nb_3C_3$ alloys melt spun at different wheel speeds: 20 m/s (□), 30 m/s (♦), 40 m/s (■), 50 m/s (×) and 60 m/s (△).

4. Conclusion

In our present research work on rapidly solidified melt-spun Sm–Co alloys, an optimum wheel speed of 50 m/s was observed. At this wheel speed relatively homogeneous and uniform microstructure with smallest (optimum) grain size (~50 nm) was observed which resulted in maximum coercivity (~4.77 kOe) as well as maximum remanence (~4.77 emu/g) for the melt-spun ribbons. The solidification parameters significantly affected the microstructures of melt-spun Sm_2Co_{17} alloys modified with Nb and C. While rapid solidification resulted in the formation of the disordered $TbCu_7$-type structure at all wheel speeds, higher wheel speeds resulted in finer grain sizes, with grain sizes varying from 150 nm at 20 m/s to 50 nm at 50 m/s. Alloys melt spun at 60 m/s contained some fcc-Co, and had a slightly coarser grain size than the alloy melt spun at 50 m/s, which was attributed to in-flight annealing. The smaller grain sizes of both (1:7) phase and Co has a slight tendency to improve the exchange–spring interactions which have been also referred in some other research work [18], but here we focused mainly on how the various wheel speed or quenching rate affected the grain size of (1:7) phase. The finer grain sizes resulted in increases in coercivity and remanence. The maximum coercivity of 4.8 kOe was observed at the finest grain size.

Acknowledgements

The authors are grateful to the National Science Foundation for support of this work under grant no. DMR0305354. Authors are grateful to the Center for Materials Research and Analysis and MRSEC: QSPINS (NSF grant no. 0213808) for facility support. Many useful discussions with L.H. Lewis, R. Skomski and R.W. McCallum are gratefully acknowledged.

References

[1] A.R. Yan, W.Y. Zhang, H.W. Zhang, B.G. Shen, Mater. Sci. Eng. B 48 (1999) 111.
[2] A.R. Yan, W.Y. Zhang, H.W. Zhang, B.G. Shen, J. Magn. Magn. Mater. 210 (2000) L10.
[3] A.R. Yan, W.Y. Zhang, H.W. Zhang, B.G. Shen, J. Appl. Phys. 88 (2000) 2787.
[4] A.R. Yan, Z. Sun, B. Han, B. Shen, J. Mater. Res. 17 (2002) 648.
[5] A.R. Yan, A. Bollero, K.H. Müller, O. Gutfleisch, J. Appl. Phys. 91 (2002) 8825.
[6] I. Panagiotopoulos, T. Matthias, D. Niarchos, J. Fidler, J. Magn. Magn. Mater. 247 (2002) 355–362.
[7] S.S. Makridis, G. Litsardakis, I. Panagiotopoulos, D. Niarchos, Y. Zhang, G.C. Hadjipanayis, IEEE Trans. Magn. 38 (2002) 2922.
[8] F. Shahri, A. Beitollahi, J. Non-Cryst. Solids 354 (14) (2008) 1487–1493.
[9] N. Hayashi, M. Daniil, Y. Zhang, G.C. Hadjipanayis, J. Alloys Compd. 305 (2000) 290–297.
[10] S. Yang, X.S. Liu, S.D. Li, G.Z. Xie, X.P. Song, B.X. Gu, Y.W. Du, Mater. Sci. Eng. A347 (2003) 325–329.
[11] X.Y. Zhang, Y. Guan, L. Yang, J.W. Zhang, Mater. Lett. 57 (2003) 2305–2309.

[12] T.V. Khoaa, D.S. Suna, N.D. Haa, S.M. Honga, H.M. Jina, Y.B. Kimc, G.W. Kima, N.P. Duongb, L.T. Tua, K.E. Leea, T.D. Hienb, L.T. Taib, C.G. Kima, C.O. Kima, J. Magn. Magn. Mater. 304 (2006) e249–e251.
[13] Z. Wang, S. Zhou, Y. Qiao, M. Zhang, R. Wang, J. Magn. Magn. Mater. 218 (2000) 72–80.
[14] Z. Wang, S. Zhou, Y. Qiao, M. Zhang, R. Wang, J. Alloys Compd. 299 (2000) 258–263.
[15] Z. Chen, Y. Zhang, G.C. Hadjipanayis, Q. Chen, B. Ma, J. Magn. Magn. Mater. 206 (1999) 8–16.
[16] Z. Chen, Y. Zhang, G.C. Hadjipanayis, Nanostruct. Mater. 11 (8) (1999) 1285–1292.
[17] Z.Q. Jin, H. Okumura, Y. Zhang, H.L. Wang, J.S. Munoz, G.C. Hadjipanayis, J. Magn. Magn. Mater. 248 (2002) 216–222.
[18] J.E. Shield, V.K. Ravindran, S. Aich, A. Hsiao, L.H. Lewis, Scripta Mater. 52 (2005) 75–78.
[19] S. Aich, J. Kostogorova, J.E. Shield, J. Appl. Phys. 97 (2005), 10H108 1-3.
[20] V.K. Ravindran, M.S. Thesis, University of Nebraska-Lincoln, 2004.
[21] J. Kostogorova-Beller, M.J. Kramer, J.E. Shield, J. Alloys Compd. 463 (2008) 207.
[22] J.E. Shield, B.E. Meacham, B.B. Kappes, K.W. Dennis, M.J. Kramer, J. Alloys Compd. 351 (2003) 106–113.
[23] J. Kostogorova-Beller, M.J. Kramer, J.E. Shield, J. Mater. Res. 23 (2008) 2886.
[24] D.M. Stefanescu, Science and Engineering of Casting Solidification, second edition, Springer, New York, 2009.
[25] K. Uestener, M. Katter, W. Rodewald, IEEE Trans. Magn. 41 (2006) 2897.
[26] C.H. Chen, S. Kodat, M.H. Walmer, V.G. Harris, J. Appl. Phys. 93 (2003) 7966.
[27] A. Yan, A. Bollero, K.H. Müller, O. Gutfleisch, J. Appl. Phys. 91 (2002) 8825.
[28] D.C. Crew, L.H. Lewis, J. Appl. Phys. 87 (2000) 4783.
[29] A. Hsiao, S. Aich, L.H. Lewis, J.E. Shield, IEEE Trans. Magn. 40 (2004) 2913.
[30] A. Yan, O. Gutfleisch, A. Handstein, T. Gemming, K.H. Müller, J. Appl. Phys. 93 (2003) 7975.